First-principles study of defect energetics in titanium-doped alumina

Katsuyuki Matsunaga and Atsutomo Nakamura
Institute of Engineering Innovation, The University of Tokyo, 2-11-16, Yayoi, Bunkyo-ku, Tokyo 113-8656, Japan

Takahisa Yamamoto
Department of Advanced Materials Science, Graduate School of Frontier Sciences, The University of Tokyo, 2-11-16, Yayoi, Bunkyo-ku, Tokyo 113-8656, Japan

Yuichi Ikuhara
Institute of Engineering Innovation, The University of Tokyo, 2-11-16, Yayoi, Bunkyo-ku, Tokyo 113-8656, Japan
(Received 7 August 2003; published 9 December 2003)

First-principles plane-wave pseudopotential calculations were performed to study electronic structures, structural relaxation, and energetics of point defects in Ti-doped Al_2O_3. Substitutional and interstitial Ti ions with charge compensating intrinsic defects were considered, and their formation energies were evaluated under various atomic chemical potentials. It was found that substitutional Ti^{4+} ions with charge compensating Al vacancies were most stable in the oxidized condition. In contrast, as oxygen chemical potentials decreased, the formation energy of substitutional Ti^{3+} decreased to have the smallest value in the relatively reduced conditions. However, in the intermediate range of oxygen potentials, substitutional Ti^{3+} and Ti^{4+} exhibited similar formation energies, indicating that these Ti defects can coexist in a particular reduction environment.

DOI: 10.1103/PhysRevB.68.214102 PACS number(s): 61.72.Bb, 61.72.Ji, 71.15.Mb

I. INTRODUCTION

Dopants and impurities in Al_2O_3 have a great influence in the high temperature properties such as plastic deformation and creep resistance.[1–4] This is because mass transport properties of Al_2O_3 are altered, as a result of a change in the point defect chemistry and its relevant diffusion properties by the presence of dopants.[5,6] In particular, since concentrations of intrinsic point defects in undoped Al_2O_3 are expected to be quite small due to their relatively high formation energies, stable point defect structures in Al_2O_3 can be controlled by adding a small amount of dopants.[7–9] Therefore, it is of great importance to understand the point-defect chemistry and the dopant effects in Al_2O_3.

Among dopants often encountered in Al_2O_3, titanium (Ti) is known to have important effects on mechanical and electrical properties of Al_2O_3. For example, Pletka *et al.* studied the high-temperature deformation behavior and the resultant dislocation structures of Ti-doped Al_2O_3 single crystals (sapphire).[1] They found that Ti^{3+}-doped Al_2O_3 exhibited a deformation behavior and dislocation substructures similar to those in undoped Al_2O_3, whereas Ti^{4+}-doped Al_2O_3 showed significant increases in the flow stresses and work-hardening rates. The difference in the results were attributed to the difference in bulk or pipe diffusion rates between Ti^{3+}- and Ti^{4+}-doped Al_2O_3, which is closely related to the kind of point defects formed in these two crystals.

In order to investigate the defect structure in Al_2O_3 doped with Ti, Monapatra *et al.* performed electrical conductivity measurements at high temperatures under different oxygen partial pressures.[7] They concluded that Ti^{4+} ions in Al_2O_3 are substituted for Al^{3+} ($Ti_{Al}{}^{1+}$), and Al vacancies ($V_{Al}{}^{3-}$) are also introduced as charge compensating defects, namely $\{3Ti_{Al}{}^{1+}:V_{Al}{}^{3-}\}$. Additionally, they reported that a certain proportion of Ti^{4+} ions was reduced to Ti^{3+}, to increase the electronic conductivity, as oxygen partial pressures for the Ti-doped Al_2O_3 system were lowered. Since Ti^{3+} ions have an electronic configuration of $[Ar]3d^1$ and are isovalent with Al^{3+}, it is expected that the Ti^{3+} ions in Al_2O_3 ($=Ti_{Al}{}^{0}$) formed in the reduced atmosphere can induce donorlike levels in the band gap without any charge compensating defects, which can contribute to the electronic conduction. In our recent study, it was also found that Ti nanowires were successfully produced using dislocations in deformed Al_2O_3, and they exhibited an extremely high electronic conductivity even at room temperature.[10] From the experimental electron energy loss spectra, the Ti nanowires were mainly composed of substitutional Ti^{4+} ions dissolving at the vicinity of dislocations in Al_2O_3. However, the Ti nanowires are expected to contain a certain amount of Ti^{3+} ions as well as Ti^{4+}, which can give rise to the unusual electric conductivity observed. It can be said, therefore, that the stable defect structure in Ti-doped Al_2O_3 is very sensitive to chemical environment of the system, and plays a crucial role for the interesting mechanical and electrical properties.

Because of the importance of the defect structure in Ti-doped Al_2O_3, a number of researches have focused on the energetics of point defects in undoped and Ti-doped Al_2O_3, mainly using atomistic simulations based on empirical or semiempirical ionic potentials.[9,11,12] Although the researches provided detailed information on theoretical defect energies and stable defect structures such as clustering of dopant ions and intrinsic defects, they did not explicitly take account the chemical environment that the system actually undergoes. As mentioned before, the Ti-doped Al_2O_3 system exhibits different properties depending on valence states of Ti ions that vary with the atmosphere surrounding the system. In such a case, it is required to study the point defect chemistry in Ti-doped Al_2O_3 under various chemical environments in detail.

The purpose of this study is to perform first-principles pseudopotential calculations for understanding point defect structures in Ti-doped Al_2O_3. In the calculations, electronic and atomic structures of possible defect species in Ti-doped Al_2O_3 were calculated, using large supercells. In addition, the dependence of defect formation energies on atomic chemical potentials in Ti-doped Al_2O_3 was investigated, applying the well-established formalism for point defect energetics from total energy calculations.[13] The obtained results were discussed with previous experimental results regarding the defect structures and its related properties in Ti-doped Al_2O_3.

II. COMPUTATIONAL PROCEDURE

First-principles pseudopotential calculations were performed within the generalized gradient approximation (GGA) using the Perdew-Wang exchange-correlation potential,[14] as implemented in the VASP code.[15,16] In the present bulk and supercell calculations, wave functions were expanded in a plane-wave basis set with a plane-wave cutoff energy (E_{cut}) of 500 eV, and it was confirmed that the total energies of aluminum and titanium oxides were converged within 1.2 meV/atom for the total energies obtained at 700 eV. For structure optimization, atoms were allowed to relax, using a conjugate gradient technique, until their residual forces were less than 0.1 eV/Å.

A. Pseudopotentials and bulk calculations

For Ti and O, ultrasoft Vanderbilt-type pseudopotentials were used, as supplied by the authors of Refs. 17 and 18. The O pseudopotential was generated from the $2s^2 2p^4$ electronic configuration with a core radius of 1.55 a.u. The reference configuration for the Ti pseudopotential was $[\mathrm{Ar}]3d^3 4s^1$, with a core radius of 2.79 a.u. and the $3d$ and $4s$ electrons were considered as valence states. In contrast, the soft norm-conserving pseudopotential by the Rappe-Rabe-Kaxiras-Joannopoulos scheme[19] was used for Al, which was generated in the $3s^2 3p^1$ configuration and a core radius was taken to be 1.82 a.u. Partial core correction was included in these Ti and Al pseudopotentials.

Using the above pseudopotentials, bulk structures relevant to the Ti-Al_2O_3 system were calculated to ensure applicability and accuracy of the pseudopotentials. In this case, the following crystals were considered: Al (fcc, $Fm3m$), Al_2O_3 (corundum, $R\bar{3}c$), Al_2TiO_5 (pseudobrookite, $Bbmmm$), TiO_2 (rutile, $P4_2/mnm$), Ti_2O_3 (corundum, $R\bar{3}c$), TiO (rocksalt, $Fm3m$ and monoclinic, $A2/m$), and metallic Ti (hcp, $P6_3/mmc$).[20–26] It is noted here that in addition to the usual rocksalt structure of TiO, the monoclinic phase of TiO, experimentally found at a high temperature, was taken into account, in which cation and anion vacancies are ordered in the underlying rocksalt lattice, keeping the stoichiometry.[25] This phase contains five TiO molecules in the primitive cell. Leung *et al.* previously carried out first-principles pseudopotential calculations of a number of possible TiO structures, and showed that this monoclinic phase was most stable, even compared to the rocksalt structure.[27] Using a sufficient number of k points generated by the Monkhorst-Pack scheme for Brillouin-zone integrations, stable structural parameters for respective crystals were obtained by optimization of unit-cell volumes and internal atomic positions. Table I shows the calculated lattice parameters and internal coordinates for respective crystals, together with available experimental data. It can be seen that the calculated lattice parameters reasonably agreed with experiment, within an error of $\pm 3.5\%$.

Moreover, heats of formation (ΔH_f) for metal oxides containing Al and/or Ti ($M_xN_yO_z$, M and N = Al or Ti) were calculated from the total energies per molecular unit ($E_{\mathrm{tot,mol}}$) by

$$\Delta H_f^{M_xN_yO_z} = E_{\mathrm{tot,mol}}(M_xN_yO_z) - xE_{\mathrm{tot,mol}}(M) - yE_{\mathrm{tot,mol}}(N) - \frac{z}{2}E_{\mathrm{tot,mol}}(O_2). \quad (1)$$

Here $E_{\mathrm{tot,mol}}(O_2)$ indicates the total energy of molecular oxygen, which was obtained from the supercell calculation at the Γ point for an isolated O_2 molecule in a cubic cell with the dimension of $15\times15\times15$ Å^3. Table II lists the calculated ΔH_f values for the metal oxides and their experimental values at 298 K.[28,29] Among these oxides, Al_2O_3 was found to be most stable, and the relative stability of the metal oxides obtained in this study was in good agreement with the trend of the experimental data. For TiO, the calculated ΔH_f value for the monoclinic phase was smaller than that for the rocksalt phase, which is more comparable with the experimental value. This result is also consistent with the previous first-principles calculations of TiO by Leung *et al.*[27] Therefore, the monoclinic phase of TiO was selected to determine atomic chemical potentials in an equilibrium condition of the Al-Ti-O system that are necessary to calculate formation energies of defects, as will be shown below.

B. Supercells and defect formation energies

In order to calculate formation energies of Ti ions and their related point defects in Al_2O_3, 120-atom supercells of Al_2O_3 with a hexagonal shape were constructed using the optimized structure of the unit cell (see Table I), with dimensions of $a_0 = 9.58$ Å and $c_0 = 13.08$ Å. The Al_2O_3 supercell is almost the same as that used in our previous study,[8] but the cell dimensions are slightly different, due to the different set of pseudopotentials used. For calculations of substitutional Ti ions, an Al atom at around the center of the supercell was replaced by a Ti atom, while a Ti atom was put into the supercell in the case of Ti interstitial, where the normally vacant octahedral site in the Al sublattice of the corundum structure was considered as a possible interstitial site. In the supercell calculations, atoms located within a radius of 3.4 Å from a defect were allowed to relax. In this radius for relaxation, atoms within third nearest neighbor (3rdNN) sites are present for substitutional Ti, while those within 4thNN sites for Ti interstitial. Numerical integrations over Brillouin zone were performed only at the Γ point because of the large size of supercells. Intrinsic vacancies and interstitials of Al and O were also calculated using supercells in a similar manner.

TABLE I. Calculated structural parameters of materials related to the Al-Ti-O system and their comparison with experimental results. The definitions of the parameters for these materials are given in the respective references.

Oxide	Space group	Calculation	Experiment	Reference
Al	$Fm3m$	$a=4.032$ Å	$a=4.05$ Å	20
Al_2O_3	$R\bar{3}c$	$a=4.790$ Å, $c=13.076$ Å	$a=4.765$ Å, $c=13.011$ Å	21
		$u(\mathrm{Al})=0.352$, $u(\mathrm{O})=0.306$	$u(\mathrm{Al})=0.352$, $u(\mathrm{O})=0.306$	
Al_2TiO_5	$Bbmm$	$a=9.442$ Å, $b=9.794$ Å	$a=9.429$ Å, $b=9.636$ Å	22
		$c=3.600$ Å	$c=3.591$ Å	
		$x(\mathrm{Ti})=0.183$	$x(\mathrm{Ti})=0.1852$	
		$x(\mathrm{Al})=0.140$, $y(\mathrm{Al})=0.555$	$x(\mathrm{Al})=0.1346$, $y(\mathrm{Al})=0.5616$	
		$x_1(\mathrm{O})=0.765$	$x_1(\mathrm{O})=0.7575$	
		$x_2(\mathrm{O})=0.043$, $y_2(\mathrm{O})=0.116$	$x_2(\mathrm{O})=0.0484$, $y_2(\mathrm{O})=0.1170$	
		$x_3(\mathrm{O})=0.312$, $y_3(\mathrm{O})=0.066$	$x_3(\mathrm{O})=0.3133$, $y_3(\mathrm{O})=0.0719$	
TiO_2	$P4_2/mnm$	$a=4.657$ Å, $c=2.980$ Å	$a=4.594$ Å, $c=2.958$ Å	23
		$u(\mathrm{O})=0.305$	$u(\mathrm{O})=0.305$	
Ti_2O_3	$R\bar{3}c$	$a=5.105$ Å, $c=14.094$ Å	$a=5.158$ Å, $c=13.611$ Å	24
		$u(\mathrm{Al})=0.345$, $u(\mathrm{O})=0.316$	$u(\mathrm{Al})=0.345$, $u(\mathrm{O})=0.311$	
TiO	$Fm3m$	$a=4.287$ Å	$a=4.177$ Å	25
TiO	$A2/m$	$a=5.872$ Å, $b=9.367$ Å	$a=5.855$ Å, $b=9.340$ Å	26
		$c=4.154$ Å, $\gamma=107°.5$	$c=4.142$ Å, $\gamma=107°.32$	
		$[x_1(\mathrm{Ti}),y_1(\mathrm{Ti})]=(0.168,0.335)$	$[x_1(\mathrm{Ti}),y_1(\mathrm{Ti})]=(0.170,0.340)$	
		$[x_2(\mathrm{Ti}),y_2(\mathrm{Ti})]=(0.677,0.349)$	$[x_2(\mathrm{Ti}),y_2(\mathrm{Ti})]=(0.669,0.342)$	
		$[x_3(\mathrm{O}),y_3(\mathrm{O})]=(0.346,0.170)$	$[x_3(\mathrm{O}),y_3(\mathrm{O})]=(0.343,0.175)$	
		$[x_4(\mathrm{O}),y_4(\mathrm{O})]=(0.829,0.170)$	$[x_4(\mathrm{O}),y_4(\mathrm{O})]=(0.833,0.179)$	
Ti	$P6/mmc$	$a=2.938$ Å, $c=4.612$ Å	$a=2.95$ Å, $c=4.68$ Å	20

Formation energies of Ti solutes and intrinsic defects in Al_2O_3 were calculated from total energies of the perfect and defective Al_2O_3 supercells, based on the standard formalism by Zhang and Northrup.[13] The detailed formulation for intrinsic defects in Al_2O_3 can also be seen in our previous study,[8] and thus only the formulation for the case of Ti defects is shown here.

For an isolated Ti defect with a charge state of q (including its sign), its formation energy (H_f) is represented using the Fermi level (E_F) as

$$H_f = E_{\mathrm{tot}}(\mathrm{defect};q) - \{E_{\mathrm{tot}}(\mathrm{perfect}) - n_{\mathrm{Al}}\mu_{\mathrm{Al}} + \mu_{\mathrm{Ti}}\} + qE_F, \quad (2)$$

TABLE II. Experimental and calculated heats of formation for oxides in eV/atom.

Oxide system	Experiment	Calculation
Al_2O_3	-3.47[a]	-3.44
Al_2TiO_5	-3.41[b]	-3.41
TiO_2	-3.24[a]	-3.38
Ti_2O_3	-3.15[a]	-3.26
TiO(rocksalt)	-2.81[a]	-2.65
TiO(monoclinic)		-2.83

[a]Reference 28.
[b]Reference 29.

where $E_{\mathrm{tot}}(\mathrm{defect};q)$ and $E_{\mathrm{tot}}(\mathrm{perfect})$ mean total energies of the defective and defect-free supercells, and μ_α (α=Al and Ti) is the atomic chemical potential. In this equation, n_{Al} is equal to 1 for substitutional Ti, whereas $n_{\mathrm{Al}}=0$ for interstitial Ti. The situation that Ti^{2+}, Ti^{3+}, and Ti^{4+} ions dissolve in Al_2O_3 was considered in this study, and thus defect charge states of $q=-1\sim+1$ were treated for substitutional Ti, while $q=+2\sim+4$ for interstitial Ti. In the case of intrinsic vacancies and interstitials in Al_2O_3, it was found in our previous study that the fully ionized charge states of the respective defect species are most stable in the entire range of chemical potentials where Al_2O_3 is stable.[8] Therefore, the fully ionized intrinsic defects of $V_{\mathrm{Al}}{}^{3-}$, $V_{\mathrm{O}}{}^{2+}$, $\mathrm{Al}_i{}^{3+}$, and $\mathrm{O}_i{}^{2-}$ were only taken into account as defects compensating the substitutional or interstitial Ti ions with effective charges. Considering the charge compensating defect reactions, neutrality of the whole system is maintained, so that it is not necessary to explicitly calculate the last term of Eq. (2).

As can be seen in Eq. (2), the formation energies depend on the atomic chemical potentials. In the ternary Al-Ti-O system studied here, however, the chemical potentials of constituent atoms vary depending on equilibrium conditions between Al-Ti-O related phases. Figure 1 shows a schematic phase diagram of the Al-Ti-O system. In the present study, Ti solutes in Al_2O_3 in the dilute limit were treated, and μ_α values of the three elements were evaluated at the four points A–D, which are close to the vertices of the three phase regions around Al_2O_3. Here, it was assumed that Al_2O_3 is

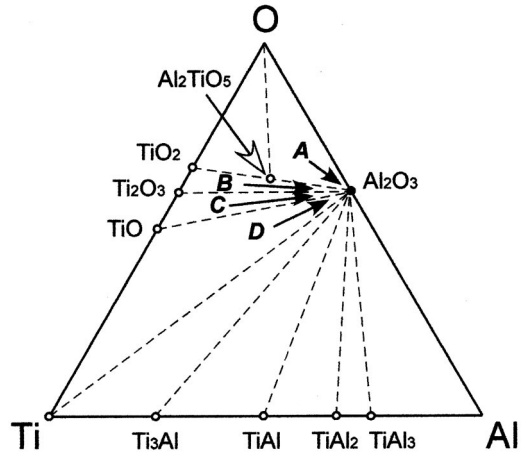

FIG. 1. Schematic illustration of the Al-Ti-O phase diagram. The points $A-D$ denoted by arrows correspond to the vertices of the three-phase region around Al_2O_3.

always stable, so that formation of metallic Al and Ti-Al phases was not taken into account. In addition, the experimental Al-Ti-O phase diagram[30,31] showed the presence of magneli phases, Ti_3O_2 and Ti_2O phases, but, for simplicity, these were not explicitly treated in this study.

From the stability of Al_2O_3, μ_{Al} and μ_O are always constrained in the following manner:

$$2\mu_{Al}+3\mu_O=\mu_{Al2O3}(\text{bulk}). \tag{3}$$

Here μ_{Al2O3}(bulk) is a total energy per molecule of perfect Al_2O_3. μ_{Al} and μ_O can vary over a range given by the heat of formation of Al_2O_3 shown in Table II. Upper bounds of μ_{Al} and μ_O can be obtained by assuming the precipitation limits of metallic Al and O_2 gas phases, i.e., $\mu_{Al} \leqslant \mu_{Al}$(bulk) and $\mu_O \leqslant \mu_O$(bulk), where μ_{Al}(bulk) and μ_O(bulk) are total energies per atom of metallic Al and molecular O_2, respectively.

At point A in Fig. 1, for example, Al_2O_3 is in equilibrium with O_2 gas and Al_2TiO_5, and thus the chemical potentials of the three elements are also constrained as

$$2\mu_{Al}+\mu_{Ti}+5\mu_O=\mu_{Al2TiO5}(\text{bulk}), \quad \mu_O=\mu_O(\text{bulk}). \tag{4}$$

Since μ_O $[=\mu_O(\text{bulk})]$ is constant through the system in this equilibrium state, μ_{Al} and μ_{Ti} can be determined by coupling Eqs. (3) and (4) as follows:

$$\mu_{Al}=\frac{1}{2}\mu_{Al2O3}(\text{bulk})-\frac{2}{3}\mu_O(\text{bulk}), \tag{5}$$

$$\mu_{Ti}=\mu_{Al2TiO5}(\text{bulk})-\mu_{Al2O3}(\text{bulk})-2\mu_O(\text{bulk}). \tag{6}$$

By using Eqs. (5) and (6), the formation energy of a Ti solute at the equilibrium point A is obtained from Eq. (2).

In a similar way, the μ_α values can be determined at the respective points under the following correlations, together with Eq. (3):

Point B: $2\mu_{Al}+\mu_{Ti}+5\mu_O=\mu_{Al2TiO5}(\text{bulk})$,

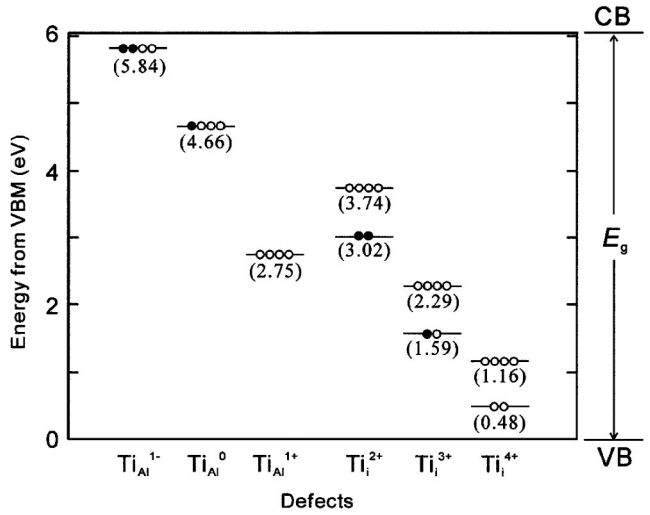

FIG. 2. One-electron energy level diagrams around the band gap (E_g) for substitutional and interstitial Ti ions obtained by the present supercell calculations. Solid circles indicate electrons occupying the levels, while open circles holes. The valence band maximum is set at 0 eV, and the theoretical E_g value (6.04 eV) is employed.

$$2\mu_{Ti}+3\mu_O=\mu_{Ti2O3}(\text{bulk}). \tag{7}$$

Point C: $\mu_{Ti}+\mu_O=\mu_{TiO}(\text{bulk})$,

$$2\mu_{Ti}+3\mu_O=\mu_{Ti2O3}(\text{bulk}). \tag{8}$$

Point D: $\mu_{Ti}+\mu_O=\mu_{TiO}(\text{bulk})$, $\quad \mu_{Ti}=\mu_{Ti}(\text{bulk})$. (9)

It is noted that the μ(bulk) values of the reference materials were total energies obtained after structural optimization, which was described in Sec. II A.

III. RESULTS AND DISCUSSION

A. Electronic structures of Ti solutes

Figure 2 shows schematic illustrations of the highest-occupied and/or lowest-unoccupied one-electron states within the band gap for substitutional (Ti_{Al}^q) and interstitial Ti ions (Ti_i^q) with various charge states. In this figure, the band-gap width (E_g) corresponds to a theoretical value (6.04 eV) for perfect Al_2O_3 obtained in the present supercell calculation. The theoretical E_g value is underestimated as compared to experimental values (8.7 eV for Al_2O_3),[32,33] but this is a common feature of GGA calculations used in this study. Numerical values depicted in parentheses indicate energy positions of the bands measured from the valence band maximum (VBM).

It can be seen from Fig. 2 that for Ti_{Al}^q and Ti_i^q defects, extra levels are present in the band gap. In the case of substitutional Ti ions (Ti_{Al}^q), the extra levels are located almost beyond $E_g/2$. The extra level at 4.66 eV for Ti_{Al}^0 ($=Ti^{3+}$ at the Al site) is occupied by one electron, while that at 5.84 eV for Ti_{Al}^{1-} ($=Ti^{2+}$ at the Al site) has two electrons. For example, a contour plot of squares of the wave function for Ti_{Al}^0 on the {1120} plane of the corundum structure is indi-

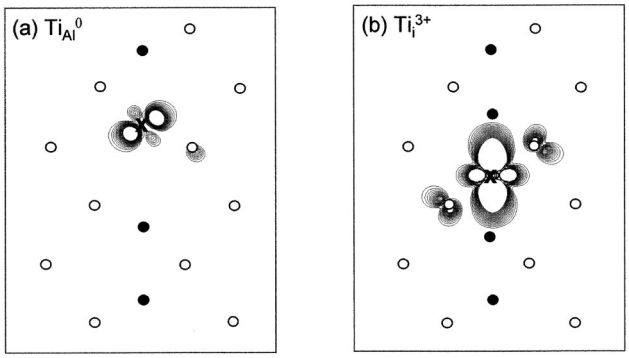

FIG. 3. Contour maps of the wave functions of Ti-induced defect levels on an $\{11\bar{2}0\}$ plane of the corundum structure. The contour lines are from 0.04 to 0.2 with an interval of 0.01 in the unit of electrons/Å^3. Solid and open circles indicate positions of Al and O ions, respectively. The position of Ti is represented by *X*.

cated in Fig. 3(a). The wave function is mainly composed of Ti-3*d* orbitals, and is strongly localized at the Ti_{Al} site. It can be said, therefore, that this level is induced by the presence of Ti_{Al}^{0}, and corresponds to a ''defect level.'' Mohapatra *et al.* experimentally studied the energy position of the defect level for Ti_{Al}^{0} from the optical data, and showed that the defect level was located at 4.25 eV from the conduction band minimum of Al_2O_3.[7] If the E_g value of perfect Al_2O_3 is taken to be an experimental value of 8.7 eV,[34–35] the energy position of the defect level can be estimated to be 4.45 eV from the VBM, which agrees well with the energy position for Ti_{Al}^{0} obtained in this study (4.66 eV). Although the theoretical E_g value for Al_2O_3 is smaller by about 3 eV than experimental data, therefore, it is thought that the energy positions of the defect levels for Ti_{Al}^{q} are well reproduced by the present calculations.

In the cases of Ti_i^{q} defects, extra levels appeared in the lower part of E_g. The Ti_i^{3+} defect has the extra level at 1.59 eV occupied by one electron, and two electrons occupy the level at 3.02 eV for Ti_i^{2+}. From the wave function for Ti_i^{3+} shown in Fig. 3(b), this level is also mainly composed of Ti-3*d* orbitals and is localized at the interstitial site, indicating the interstitial-induced defect level. It is noted that the energies of the defect levels are increased, as the charge states q of Ti interstitial decrease and more electrons occupy these levels. This tendency is the same as the case of substitutional Ti ions, and is likely due to electronic repulsions in these levels localized at the defect sites.

Since the Ti_{Al} and Ti_i defects relax surrounding ions due to their different ionic sizes and charges from Al and O, distances from a Ti defect to neighboring ions are changed. The distances after structural optimization are listed in Table III. It is noted here that atoms in a certain coordination shell from a defect are not always located at the same distance in Al_2O_3, because of the low symmetry of the corundum structure. In such a case, average values in the respective atomic coordination shells are shown in this table. Together with the results for Ti defects, this table contains the results for fully charged intrinsic vacancies and interstitials in Al_2O_3. Details on the structural relaxations for intrinsic vacancies and interstitials can also be seen in our previous paper.[8] Thus, only relaxed structures around Ti defects will be discussed in detail below.

For Ti_{Al}^{q}, the 1stNN O ions exhibit outward relaxations of more than 1.5%. This can be understood from the larger ionic sizes of Ti ions than Al ions.[34] The 2ndNN Al ions also tend to slightly move away from the Ti_{Al}^{1+} defect, due to the electrostatic repulsion between them. However, in the cases of $q=-1$ and 0, the distances between Ti_{Al}^{q} and 2ndNN Al ions are almost the same with that between Al ions in the perfect lattice.

The interstitial site of the prefect Al_2O_3 lattice is twofold coordinated by Al ions at the 1stNN sites. In the presence of Ti_i^{q}, however, it was found that the two Al ions undergo

TABLE III. Structural relaxation around each defect species. Average distances from the defect positions to neighboring atoms are listed. Neighboring atomic species and their coordination numbers are also shown in parentheses.

	Distance in Å (atomic species; coordination number)			
	1stNN	2ndNN	3rdNN	4thNN
Al site in bulk Al_2O_3	1.93(O;6)	2.78(Al;4)	3.24(Al;3), 3.24(O;3)	
Ti_{Al}^{1-}	2.05(O;6)	2.77(Al;4)	3.25(Al;3), 3.24(O;3)	
Ti_{Al}^{0}	2.01(O;6)	2.80(Al;4)	3.26(Al;3), 3.23(O;3)	
Ti_{Al}^{1+}	1.96(O;6)	2.84(Al;4)	3.29(Al;3), 3.22(O;3)	
V_{Al}^{3-}	2.06(O;6)	2.58(Al;4)	3.15(Al;3), 3.27(O;3)	
O site in bulk Al_2O_3	1.93(Al;4)	2.74(O;12)	3.24(Al;2)	
V_O^{2+}	2.11(Al;4)	2.66(O;12)	3.25(Al;2)	
Interstitial site in bulk Al_2O_3	1.93(Al;2)	1.99(O;6)	2.78(Al;6)	3.31(O;6)
Ti_i^{2+}	2.03(O;6)	2.21(Al;2)	2.88(Al;6)	3.30(O;6)
Ti_i^{3+}	1.97(O;6)	2.26(Al;2)	2.89(Al;6)	3.28(O;6)
Ti_i^{4+}	1.93(O;6)	2.30(Al;2)	2.91(Al;6)	3.26(O;6)
Al_i^{3+}	1.86(O;6)	2.25(Al;2)	2.87(Al;6)	3.28(O;6)
O_i^{2-}	1.71(Al;2)	2.26(O;6)	2.76(Al;6)	3.31(O;6)

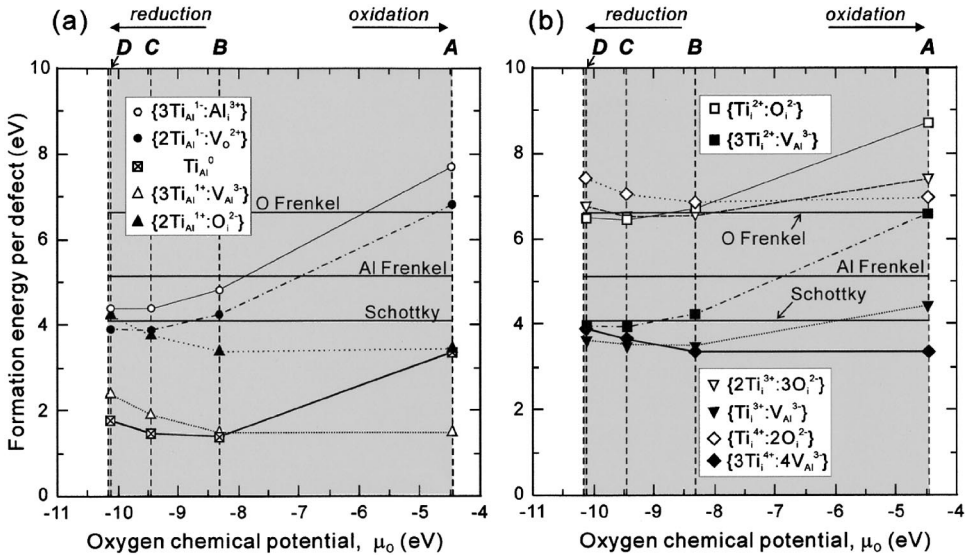

FIG. 4. Formation energies per defect of (a) substitutional and (b) interstitial Ti defects against oxygen chemical potentials (μ_O). For comparison, energies of intrinsic Schottky, Al Frenkel and O Frenkel defects are also depicted. The shaded area indicates the μ_O range where Al_2O_3 is always stable. The symbols of $A-D$ correspond to the equilibrium points shown in Fig. 1.

significant outward relaxations of more than 14%. Instead, the six O ions at the 2ndNN sites of the perfect lattice move toward Ti_i^q, and become 1stNN ions for the Ti_i^q ions. The distances of Ti_i^q and the 1stNN O ions decrease with rising defect charge q, while those from Ti_i^q to 2ndNN and 3rdNN Al ions increase. Such a trend in the distances from the Ti_i^q defects can be understood by electrostatic interactions between ions. The O^{2-} ions at the 1stNN sites are electrostatically attracted by the more positively charged Ti_i^q, and the Al^{3+} ions at the 2ndNN and 3rdNN sites move away from Ti_i^q due to their electrostatic repulsions.

It is noted that for all defect species studied here, atomic relaxations in the outermost coordination shells are at most about 1.5%. Although only atoms within a relaxation cutoff of 3.4 Å were allowed to relax in this study, it is likely that formation energies of Ti and its related defects are not affected significantly by the relaxation cutoff. In fact, it was confirmed in our previous study that the formation energies of intrinsic defects in Al_2O_3 converged to be less than 0.1 eV per defect when the cutoff radius was 3.4 Å, as compared to those obtained with a larger cutoff radius (3.6 Å).[8]

B. Defect formation energies

Figure 4 shows the calculated formation energies against oxygen chemical potentials determined from the phase equilibrium conditions in Fig. 1. Figure 4(a) indicates the formation energies of Ti_{Al}^q-related defects, while those of Ti_i^q-related defects are plotted in Fig. 4(b). In these figures, formation energies of intrinsic Schottky $\{2V_{Al}^{3-}:3V_O^{2+}\}$, Al Frenkel $\{Al_i^{3+}:V_{Al}^{3-}\}$ and O Frenkel $\{O_i^{2-}:V_O^{2+}\}$ defects are also depicted, for comparison. In the oxidation limit [at the point A, $\mu_O=\mu_O(\text{bulk})=-4.46$ eV], $\{3Ti_{Al}^{1+}:V_{Al}^{3-}\}$ was found to exhibit the smallest energy (1.44 eV), which indicates that Ti ions in Al_2O_3 have a charge state of Ti^{4+} at the Al sites with charge compensating V_{Al}^{3-} under oxidation condition. This can be imagined from the compound such as Al_2TiO_5, where Ti ions have a formal charge of +4, are in equilibrium with Al_2O_3 in the oxidation atmosphere. It can also be seen from Fig. 4(b) that Ti^{4+} ions at the interstitial sites with charge compensating V_{Al}^{3-} and O_i^{2-} have larger formation energies, indicating that Ti^{4+} ions favorably dissolve at the Al sites in Al_2O_3.

Previous experimental and atomistic-simulation studies pointed out the possibility of clustering of Ti_{Al}^{1+} and V_{Al}^{3-}.[9,11] This may be due to electrostatic and elastic interactions between the two defect species. In order to address this issue, separate calculations using supercells containing $\{Ti_{Al}^{1+}:V_{Al}^{3-}\}^{2-}$ complexes were also carried out. In this case, two defect configurations were considered; V_{Al}^{3-} is located at the 2ndNN or 3rdNN Al site from substitutional Ti^{4+}. As can be seen from Table II, distances between Ti_{Al}^{1+} and V_{Al}^{3-} in the two defect configurations are 2.78 and 3.24 Å before atomic relaxation, respectively. In the similar way to the calculations for isolated defects, atoms located within 3.4 Å from each defect species were allowed to relax. It was found that a total energy difference of $E_{tot}(\text{2ndNN configuration})-E_{tot}(\text{3rdNN configuration})$ is -0.85 eV. This indicates that Ti_{Al}^{1-} and V_{Al}^{3-} tend to be located more close to each other, resulting in the clustering of these defects.

When the μ_O values decrease from μ_O(bulk) in Fig. 4, a number of defect formation energies tend to decrease. It should be noted here that Ti_{Al}^0 becomes more stable with decreasing μ_O, and the formation energy at point B is as small as that of $\{3Ti_{Al}^{1+}:V_{Al}^{3-}\}$. Moreover, the Ti_{Al}^0 defects become most stable in the further reduction conditions such as points C and D. Since Ti_2O_3 is in equilibrium with Al_2O_3 at these reduction conditions (see Fig. 1), Ti ions in Al_2O_3 are considered to also have a charge state of +3 in the reduction atmosphere. As can be seen from Fig. 4(b), interstitial Ti^{3+} ions with charge compensating V_{Al}^{3-} and O_i^{2-} defects exhibit much larger energies than Ti_{Al}^0, and thus Ti^{3+} ions at the interstitial sites are not energetically favorable.

In the case of Ti^{2+}-related defects, their formation energies are much higher over the entire range of μ_O, as compared to those of Ti^{3+}- and Ti^{4+}-related defects. It can be said that Ti ions in Al_2O_3 have charge states of +3 or +4,

TABLE IV. Concentrations of substitutional Ti^{3+} and Ti^{4+} ions at each equilibrium point of the phase diagram (Fig. 1), calculated at 1600 K.

Equilibrium point	$[Ti_{Al}^{0}]$ (cm^{-3})	$[Ti_{Al}^{1+}]$ (cm^{-3})	$[Ti_{Al}^{0}]/([Ti_{Al}^{0}]+[Ti_{Al}^{1+}])$
A	1.05×10^{12}	1.00×10^{18}	1.05×10^{-6}
B	1.24×10^{18}	1.00×10^{18}	5.53×10^{-1}
C	1.24×10^{18}	4.67×10^{16}	9.64×10^{-1}
D	1.05×10^{17}	1.15×10^{15}	9.89×10^{-1}

and can stably dissolve at the Al sites. It is also noted that the formation energies of the substitutional Ti^{3+} and Ti^{4+} defects are much smaller than those of the intrinsic defects, and thus the stable defect structures in Al_2O_3 are greatly affected by the presence of Ti ions, which was also pointed out by Lagerlöf *et al.*[9]

In the reduction conditions of the points *B*, *C*, and *D*, the formation energy of Ti_{Al}^{0} is the smallest, and yet is still close to that of $\{3Ti_{Al}^{1+}:V_{Al}^{3-}\}$. This suggests that a certain amount of Ti ions in Al_2O_3 may have a charge state of $+4$ even in the reduction conditions. Based on the results of the formation energies shown in Fig. 4, therefore, equilibrium defect concentrations ($[D]$) of Ti_{Al}^{0} and Ti_{Al}^{1+} ions in Al_2O_3 were estimated using the formalism by Zhang *et al.*[13] and Van de Walle *et al.*,[35] as follows:

$$[D]=N_{\text{sites}}\exp\left(-\frac{H_f}{k_BT}\right). \tag{10}$$

Here, N_{sites} is the number of sites per unit volume of the Al_2O_3 crystal where defects can be present. In this case, Ti_{Al}^{0}, Ti_{Al}^{1+}, and V_{Al}^{3-} defects are situated at the Al sites, so that N_{site} corresponds to the number of Al sites ($=4.62\times10^{22}$ cm^{-3}) in Al_2O_3. k_B is the Boltzmann constant, and T is the temperature. In general, the energy term in Eq. (10) should be given by a Gibbs free energy, which includes terms of changes in vibrational entropy and volume due to introduction of defects. It is likely, however, that the changes in entropy for different defects are of the same order, and thus the entropy term will be negligibly small, comparing with different defects.[36] In addition, the contribution from volume change is expected to be relatively small in the case of dilute defects in solids. In Eq. (10), therefore, only the formation entalpy term was taken into account to calculate $[D]$ values.

Considering the charge-compensating defects of $\{3Ti_{Al}^{1+}:V_{Al}^{3-}\}$, concentrations of the two defect species are also correlated by the relation $[Ti_{Al}^{1+}]=3[V_{Al}^{3-}]$, due to charge-neutrality requirement of the whole system. Combining this relation with the total defect concentration for $\{3Ti_{Al}^{1+}:V_{Al}^{3-}\}$ from Eq. (10), $[Ti_{Al}^{1+}]$ values can be obtained. The $[Ti_{Al}^{0}]$ and $[Ti_{Al}^{1-}]$ values and the resultant $[Ti_{Al}^{0}]$ ratios thus obtained are listed in Table IV, where the temperature was selected at 1600 K. It is noted here that the concentrations of $[Ti_{Al}^{0}]$ and $[Ti_{Al}^{1-}]$ varied with different temperatures, but the $[Ti_{Al}^{0}]$ ratios were confirmed to be almost unchanged. As can be seen, in the oxidation-limit condition (point *A*), the concentration of Ti_{Al}^{0} is quite small, while Ti_{Al}^{0} are abundant at points *C* and *D* (the reduced conditions). However, $[Ti_{Al}^{0}]$ and $[Ti_{Al}^{1+}]$ exhibit similar values at point *B*, indicating the mixture of substitutional Ti^{3+} and Ti^{4+} defects in the intermediate μ_O condition.

Mohapatra *et al.* studied the optical absorption and electrical conductivity of Ti-doped Al_2O_3, and found that the electronic conductivity increased with decreasing oxygen partial pressure, while the ionic conductivity gradually decreased.[7] This was attributed to the formation of Ti_{Al}^{0} reduced from Ti_{Al}^{1+}, which can act as a donor-like defect having an electron within the band gap of Al_2O_3, as shown in Fig. 2. It can be said, therefore, that Al_2O_3 doped with Ti contains both Ti^{3+} and Ti^{4+} ions under a moderately low oxygen partial pressure, which is consistent with our results shown in Fig. 4 and Table IV.

In contrast, Phillips *et al.* and their co-workers discussed defect structures in Ti^{4+}-doped Al_2O_3 from observations of the dislocation structures and motion at high temperatures.[37–39] Their samples contained TiO_2 (rutile) precipitates with a needlelike shape, and dislocation loops were found to be formed from the Al_2O_3/TiO_2 interfaces. They suggested that the growth of the dislocation loops into the Al_2O_3 region were due to diffusion of oxygen interstitials accompanied with Ti^{4+} in Al_2O_3. It can be clearly seen from Fig. 4(a), however, that the formation energy of $\{2Ti_{Al}^{1+}:O_i^{2-}\}$ is much larger than that of $\{3Ti_{Al}^{1+}:V_{Al}^{3-}\}$. Thus it is not plausible that O interstitials are present as charge-compensating defects for Ti^{4+} in bulk Al_2O_3. It should be mentioned here that there is a possibility that stable defect structures around dislocations may be different from those in the bulk, which is probably due to the particular chemical environment at the vicinity of dislocations. It is well known that elastic fields of dislocations coming from their lattice discontinuity can bring about segregation of solute atoms and rapid pipe diffusion. This suggests that the point defect chemistry will also be affected by the presence of dislocations, which should be taken into account in future work.

The present results showed that the stable defect structures are different in Ti-doped Al_2O_3, depending on chemical environment, due to variations of valence states of Ti ions. In order to control high-temperature properties of ceramics, significant experimental efforts for optimizing processing parameters such as temperatures, types and amounts of dopants have been made so far. For effective materials design, however, it is necessary to fully understand defect structures due to dopants in ceramics. In this regard, the present results demonstrate the applicability of the first-principles method to obtain a detailed knowledge of the point defect chemistry in ceramic materials.

IV. SUMMARY

First-principles pseudopotential calculations were performed to study electronic structures and formation energies of point defects in Ti-doped Al_2O_3. The results obtained in this study can be summarized as follows.

(1) When Ti ions were present at the Al site or the interstitial site, extra bands appeared within the band gap of Al_2O_3. The extra bands were mainly composed of Ti-3*d* orbitals, and were strongly localized around the Ti sites.

(2) Various charge states for Ti_{Al}^{q} (substitutional) and Ti_i^{q} (interstitial) were considered, and their formation energies were systematically calculated. It was found that Ti_i^{q} defects with any charge compensating intrinsic defects exhibited much higher formation energies than Ti_{Al}^{q}-related defects, indicating that substitutional Ti defects are energetically favorable in Al_2O_3.

(3) In the oxidation condition, Ti_{Al}^{1+} with charge compensating V_{Al}^{3-} was most stable. In contrast, the formation energy of Ti_{Al}^{0} decreased with decreasing oxygen chemical potentials (μ_O). As a result, the formation energies of Ti_{Al}^{0} and Ti_{Al}^{1+} with V_{Al}^{3-} were almost the same in the intermediate μ_O condition. It can be thus said that both substitutional Ti^{3+} and Ti^{4+} ions can coexist in Al_2O_3 under a particular reduced chemical environment.

ACKNOWLEDGMENTS

This work was supported by Special Coordination Funds and a Grant-in-Aid for Scientific Research from the Ministry of Education, Culture, Sports, Science and Technology of the Japanese government. The authors also acknowledge Dr. S. Kitaoka at the Japan Fine Ceramics Center for a valuable discussion on the thermodynamics of the Al-Ti-O system.

[1] B. J. Pletka, T. E. Mitchell, and A. H. Heuer, Acta Metall. **30**, 147 (1982).
[2] H. Yoshida, Y. Ikuhara, and T. Sakuma, J. Mater. Res. **13**, 2597 (1998).
[3] H. Yoshida, Y. Ikuhara, and T. Sakuma, Philos. Mag. Lett. **79**, 249 (1999).
[4] H. Yoshida, T. Yamamoto, Y. Ikuhara, and T. Sakuma, Philos. Mag. A **82**, 511 (2002).
[5] A. H. Heuer and K. P. D. Lagerlöf, Philos. Mag. Lett. **79**, 619 (1999).
[6] K. P. D. Lagerlöf, T. E. Mitchell, and A. H. Heuer, J. Am. Ceram. Soc. **72**, 2159 (1989).
[7] S. K. Mohapatra and F. A. Kröger, J. Am. Ceram. Soc. **60**, 381 (1977).
[8] K. Matsunaga, T. Tanaka, T. Yamamoto, and Y. Ikuhara, Phys. Rev. B **68**, 085110 (2003).
[9] K. P. D. Lagerlöf and R. W. Grimes, Acta Mater. **46**, 5689 (1998).
[10] A. Nakamura, K. Matsunaga, J. Tohma, T. Yamamoto, and Y. Ikuhara, Nature Materilas **7**, 453 (2003).
[11] R. W. Grimes, J. Am. Ceram. Soc. **77**, 378 (1994).
[12] J. H. Harding, K. J. W. Atkinson, and R. W. Grimes, J. Am. Ceram. Soc. **86**, 554 (2003).
[13] S. B. Zhang and J. E. Northrup, Phys. Rev. Lett. **67**, 2339 (1991).
[14] J. P. Perdew, J. A. Chevary, S. H. Vosko, K. A. Jackson, M. R. Pederson, D. J. Singh, and C. Fiolhais, Phys. Rev. B **46**, 6671 (1992).
[15] G. Kresse, Ph.D. thesis, Technische Universität Wien, 1993.
[16] G. Kresse and J. Furthmüller, Comput. Mat. Sci. **6**, 15 (1996).
[17] D. Vanderbilt, Phys. Rev. B **41**, 7892 (1990).
[18] G. Kresse and J. Hafner, J. Phys.: Condens. Matter **6**, 8245 (1994).
[19] A. M. Rappe, K. M. Rabe, E. Kaxiras, and J. D. Joannopoulos, Phys. Rev. B **41**, 1227 (1990).
[20] C. Kittel, *Introduction to Solid State Physics*, 6th ed. (Wiley, New York, 1986).
[21] H. d'Amour, D. Schiferl, W. Denner, H. Schulz, and W. B. Holzapfer, J. Appl. Phys. **49**, 4411 (1978).
[22] B. Morosin and R. W. Lynch, Acta Crystallogr., Sect. B: Struct. Crystallogr. Cryst. Chem. **28**, 1040 (1972).
[23] S. C. Abrahams and J. L. Bernstein, J. Chem. Phys. **55**, 3206 (1971).
[24] M. G. Vincent, K. Yoon, A. Grüttner, and J. Ashkenazi, Acta Crystallogr., Sect. A: Cryst. Phys., Diffr., Theor. Gen. Crystallogr. **36**, 803 (1980).
[25] M. E. Straumanis and H. W. Li, Z. Anorg. Allg. Chem. **305**, 143 (1960).
[26] D. Watanabe, J. R. Castles, A. Jostson, and A. S. Malin, Acta Crystallogr. **23**, 307 (1967).
[27] C. Leung, M. Weinert, P. B. Allen, and R. M. Wentzcovitch, Phys. Rev. B **54**, 7857 (1996).
[28] M. W. Chase, Jr., *NIST-JANAF Themochemical Tables*, 4th ed. [J. Phys. Chem. Ref. Data, Monograph **9**, 1 (1998)].
[29] I. Barin, *Thermochemical Data of Pure Substances* (Weinheim, New York, 1989).
[30] X. L. Li, R. Hillel, F. Teyssandier, S. K. Choi, and F. J. J. van Loo, Acta Metall. Mater. **40**, 3149 (1992).
[31] G. P. Kelkar and A. H. Carim, J. Am. Ceram. Soc. **78**, 572 (1995).
[32] R. H. French, J. Am. Ceram. Soc. **73**, 477 (1990).
[33] M. L. Boltz and R. H. French, Appl. Phys. Lett. **55**, 1955 (1989).
[34] R. D. Shannon, Acta Crystallogr., Sect. A: Cryst. Phys., Diffr., Theor. Gen. Crystallogr. **32**, 751 (1976).
[35] C. G. Van de Walle, D. B. Larks, G. F. Neumark, and S. T. Pantelides, Phys. Rev. B **47**, 9425 (1993).
[36] A. F. Kohan, G. Ceder, D. Morgan, and C. G. Van de Walle, Phys. Rev. B **61**, 15 019 (2000).
[37] D. S. Phillips, A. H. Heuer, and T. E. Mitchell, Philos. Mag. A **42**, 385 (1980).
[38] D. S. Phillips, A. H. Heuer, and T. E. Mitchell, Philos. Mag. A **42**, 405 (1980).
[39] D. S. Phillips, T. E. Mitchell, and A. H. Heuer, Philos. Mag. A **42**, 417 (1980).